Non-orthogonal frequency-division multiplexing based on eigenvalue decomposition

Seichiroh Osaki [1], Takumi Ishihara [1], and Shinya Sugiura [2]

[1]Affiliation not available
[2]The University of Tokyo

October 30, 2023

Abstract

Postprint accepted on 21 May 2020 for publication in IEEE 92nd Vehicular Technology Conference. (c)2020 IEEE. Personal use of this material is permitted. Permission from IEEE must be obtained for all other uses, in any current or future media, including reprinting/republishing this material for advertising or promotional purposes, creating new collective works, for resale or redistribution to servers or lists, or reuse of any copyrighted component of this work in other works.

Non-Orthogonal Frequency-Division Multiplexing Based on Eigenvalue Decomposition

Seichiroh Osaki
Tokyo University of Agriculture and Technology

Takumi Ishihara and Shinya Sugiura*
The University of Tokyo
E-mail: sugiura@iis.u-tokyo.ac.jp

***Abstract*—This paper proposes a novel ultra-dense non-orthogonal frequency-division multiplexing (NOFDM) transmission, where subcarrier spacing is set significantly lower than that of OFDM. Eigenvalue-decomposition-aided precoding is conceived for eliminating the detrimental effects of NOFDM-specific inter-carrier interference and correlated noises. The classic capacity formula is extended to that supporting our precoded NOFDM scheme. Optimal power allocation (PA) is developed for maximizing the derived capacity of the proposed scheme. In analytical and numerical results, we demonstrate that the proposed NOFDM scheme with optimal PA outperforms the conventional NOFDM and the classic OFDM schemes.**

I. Introduction

Non-orthogonal resource allocation in the frequency domain has been developed in several different contexts, such as non-orthogonal frequency-division multiplexing (NOFDM) [1, 2], generalized frequency-division multiplexing (GFDM) [3], and spectrally efficient frequency-division multiplexing (SEFDM) [4, 5], in contrast to the classic orthogonal frequency-division multiplexing (OFDM) counterpart [6]. In NOFDM, by allowing the introduction of inter-carrier interference (ICI) between non-orthogonally overlapped subcarriers, further flexible resource allocation becomes realistic. In addition to the scenario of microwave communications, NOFDM was experimentally investigated in the context of the optical fiber communications [7, 8], the visible light communications [9], and the E-band wireless transmission [10]. In [11], the precoded NOFDM scheme was presented for decoupling ICI effects between substreams, while any power allocation (PA) onto each substream is not incorporated. However, information-theoretic analysis of the explicit merits attained by NOFDM has not been well investigated. The only exception is that constituted in [12], where the potential capacity gain of NOFDM was shown without any precoding and PA.

Time-domain resource allocation has been developed as faster-than-Nyquist (FTN) signaling, which relies on the transmission of non-orthogonal pulses whose interval is shorter than that defined by the inter-symbol interference (ISI)-free Nyquist criterion. The theoretical information rate of unprecoded FTN signaling was analyzed in [13], where the performance gain of the FTN signaling scheme over the Nyquist-based counterpart was attained owing to the exploitation of the excessive bandwidth under the assumption of the use of a root raised cosine (RRC) shaping filter. However, the benefits of FTN signaling over the Nyquist counterpart were not clarified in the absence of the excess bandwidth. Several low-complexity detection algorithms were developed for equalizing the ISI-contaminated FTN symbols at the receiver [14–16].

Most recently, in [17], singular value decomposition (SVD)-precoded FTN signaling with optimal and truncated PA was proposed, where the classic Shannon limit is extended to that supporting non-orthogonal symbol transmissions in the time domain. However, in general, the unprecoded and precoded FTN signaling schemes typically assume block transmissions, and the rate loss induced due to inter-block interference is unavoidable. However, in most previous studies, the benefits of FTN signaling were verified by ignoring the inter-block interference (IBI) effects. Furthermore, in [18], the performance tradeoff between the calculation precision and the achievable information rate, specifically found in the SVD-precoded FTN signaling, was investigated.

Against this background, the novel contributions of this paper are as follows. Motivated by the recent concept of SVD-precoded FTN signaling [17], we propose a precoded ultra-dense NOFDM transmission, where the subcarrier spacing is set lower than that of OFDM. Information symbols, modulated onto non-orthogonal subcarriers, are precoded with eigenvalue decomposition (EVD) as well as linear PA. The classic capacity formula is generalized to support the proposed NOFDM, based on the ICI-free equivalent system model of NOFDM aided by EVD. The PA coefficient for each NOFDM subcarrier is optimized for maximizing the derived capacity, with the aid of the Lagrange multiplier method. Our analytical and numerical results demonstrate that the proposed precoded NOFDM scheme with optimal PA outperforms the conventional NOFDM and the classic OFDM counterparts.

II. System Model

A. System Model of Precoded NOFDM

In this section, we introduce the system model of the proposed EVD-precoded NOFDM architecture with PA. At the NOFDM transmitter, information bits are modulated onto N complex-valued symbols $\mathbf{s}_l = [s_{l,0}, \cdots, s_{l,N-1}]^T \in \mathbb{C}^N$,

Postprint accepted on 21 May 2020 for publication in *IEEE 92nd Vehicular Technology Conference*, 2020.

where l is the frame index, and N is the number of subcarriers. The power constraint of $\mathbb{E}[\mathbf{s}_l^H \mathbf{s}_l] = N$ is imposed on $\mathbf{s}_l$, where $\mathbb{E}[\cdot]$ represents the expectation operation. Then, the modulated symbol block $\mathbf{s}_l$ is linearly precoded by a complex-valued matrix $\mathbf{F} \in \mathbb{C}^{N \times N}$, in order to obtain the precoded symbol block of:

$$\mathbf{x}_l = [x_{l,0}, x_{l,1}, \cdots, x_{l,N-1}]^T \in \mathbb{C}^N \tag{1}$$
$$= \mathbf{F}\mathbf{s}_l. \tag{2}$$

The precoding matrix $\mathbf{F}$ is designed for maintaining the power constraint of $\mathbb{E}[\mathbf{x}_l^H \mathbf{x}_l] = N$. Then, the precoded symbols $\mathbf{x}_l$ are multiplied by non-orthogonal subcarriers in the lth NOFDM frame, which are placed at closer spacing than the OFDM counterpart. More specifically, given T is the frame duration, the subcarrier spacing of NOFDM is expressed as $\Delta f = \alpha/T$, where α $(0 < \alpha \leq 1)$ is a compression factor.

The modulated NOFDM signals in the time-domain are represented by

$$x(t) = \sqrt{\alpha E_0} \sum_{l=-\infty}^{\infty} \sum_{n=0}^{N-1} x_{l,n} g(t - lT) e^{j2\pi n \Delta f t}, \tag{3}$$

where $g(t) \in \mathbb{R}$ is the impulse response of a shaping filter. In the proposed NOFDM scheme, an RRC shaping filter with a roll-off factor $\beta \in \mathbb{R}$ is employed, where each subcarrier, rather than the whole bandwidth, is bandlimited. Furthermore, $E_0 \in \mathbb{R}$ is a transmit energy per subcarrier in the equivalent OFDM transmitter.

For the sake of simplicity, we consider the scenario of a single frame transmission, and hence let us denote ($s_{l,n}$, $\mathbf{s}_l$, $x_{l,n}$, $\mathbf{x}_l$) as (s_n, $\mathbf{s}$, x_n, $\mathbf{x}$) in the rest of this paper. The coefficient $\sqrt{\alpha}$ (≤ 1) in (3) is added for normalizing the transmit power of each NOFDM frame per unit bandwidth $\mathbb{E}\left[|x(t)|^2\right]$. Note that the special case of $\mathbf{F} = \mathbf{I}$ corresponds to the unprecoded NOFDM scheme, where $\mathbf{I} \in \mathbb{C}^{N \times N}$ is the identity matrix.

When considering a specific available bandwidth, the relationship between the number of subcarriers of NOFDM and that of OFDM N_{OFDM} is given by

$$N = \left\lfloor \frac{N_{\mathrm{OFDM}} - 1}{\alpha} \right\rfloor + 1. \tag{4}$$

If the available bandwidth is sufficiently wide, i.e., $N_{\mathrm{OFDM}} \gg 1$, N is approximated to $N \simeq N_{\mathrm{OFDM}}/\alpha$.

Under the assumption of the additive white Gaussian noise (AWGN) channel, the received signals are represented by

$$r(t) = x(t) + n(t) \in \mathbb{R}, \tag{5}$$

where $n(t)$ is a complex-valued AWGN with a zero mean and a noise variance of N_0. The received signals are first passed through a matched filter $g^*(-t)$, and then the filtered outputs are projected onto the NOFDM subcarriers. More specifically, the received sample corresponding to the ith subcarrier is given by

$$y_i = \int_{-\infty}^{\infty} r(t) g^*(-t) e^{-j2\pi i \Delta f t} dt \in \mathbb{C}, \tag{6}$$

which is also expressed in the block representation by

$$\mathbf{y} = [y_0, y_1, \cdots, y_{N-1}]^T \in \mathbb{C}^N \tag{7}$$
$$= \sqrt{\alpha E_0}\mathbf{H}\mathbf{x} + \boldsymbol{\eta}, \tag{8}$$
$$= \sqrt{\alpha E_0}\mathbf{H}\mathbf{F}\mathbf{s} + \boldsymbol{\eta}, \tag{9}$$

where the matrix $\mathbf{H} \in \mathbb{C}^{N \times N}$ represents the effects of ICI, whose ath-row and bth-column element is denoted by [12]

$$h_{a,b} = \int_{-\infty}^{\infty} g(t) g^*(-t) e^{j2\pi(b-a)\Delta f t} dt. \tag{10}$$

Furthermore, $\boldsymbol{\eta} = [\eta_0, \eta_1, \cdots, \eta_{N-1}]^T$ are the correlated noises, each formulated by

$$\eta_i = \int_{-\infty}^{\infty} n(t) g^*(-t) e^{-j2\pi i \Delta f t} dt. \tag{11}$$

Here, the correlation matrix of the noises is calculated by $\mathbb{E}[\boldsymbol{\eta}\boldsymbol{\eta}^H] = N_0\mathbf{H}$. Note that only in the classic OFDM case employing a rectangular pulse, the ICI matrix $\mathbf{H}$ becomes the identity matrix $\mathbf{I}$ owing to the orthogonality of subcarriers, and hence the noises $\boldsymbol{\eta}$ are uncorrelated. However, in general, NOFDM with $\alpha < 1$ suffers from the effects of correlated noises, due to the non-diagonal ICI matrix $\mathbf{H}$.

B. Proposed EVD-Precoded NOFDM With Optimal PA

In this section, we present the system model of the proposed EVD-precoded NOFDM scheme with optimal PA. Since $\mathbf{H}$ is a Toeplitz and Hermitian matrix, the ICI matrix $\mathbf{H}$ is diagonalized with the aid of EVD as follows:

$$\mathbf{H} = \mathbf{U}\boldsymbol{\Lambda}\mathbf{U}^T, \tag{12}$$

where $\mathbf{U} \in \mathbb{R}^{N \times N}$ is a real-valued unitary matrix, having the relationship of $\mathbf{U}\mathbf{U}^T = \mathbf{U}^T\mathbf{U} = \mathbf{I}$, and $\boldsymbol{\Lambda} = \mathrm{diag}\{\lambda_0, \lambda_1, \cdots, \lambda_{N-1}\} \in \mathbb{R}^{N \times N}$ is a diagonal matrix that contains N non-zero eigenvalues λ_i $(i = 0, \cdots, N-1)$, arranged in ascending order. Therefore, from (9) and (12), the received sample block is expressed by

$$\mathbf{y} = \sqrt{\alpha E_0}\mathbf{U}\boldsymbol{\Lambda}\mathbf{U}^T\mathbf{x} + \boldsymbol{\eta}. \tag{13}$$

At the transmitter, a PA coefficient $\sqrt{q_i} \in \mathbb{R}$ is multiplied by the ith information symbol s_i. Then, power-allocated symbols $\sqrt{q_i}s_i$ $(i = 0, \cdots, N-1)$ are precoded by the unitary matrix $\mathbf{U}$, which yields

$$\mathbf{x} = \mathbf{U}\mathbf{Q}\mathbf{s}, \tag{14}$$

where

$$\mathbf{Q} = \mathrm{diag}\{\sqrt{q_0}, \sqrt{q_1}, \cdots, \sqrt{q_{N-1}}\} \in \mathbb{R}^{N \times N}. \tag{15}$$

From (13) and (14), the received sample block of the proposed EVD-precoded NOFDM with PA, transmitted over the AWGN

channel, is represented by

$$\mathbf{y} = \sqrt{\alpha E_0}\mathbf{U}\mathbf{\Lambda}\mathbf{Q}\mathbf{s} + \boldsymbol{\eta}. \tag{16}$$

Then, the weighs of $\mathbf{U}^T$ are multiplied by the received sample block $\mathbf{y}$ as follows:

$$\mathbf{y}_{\mathrm{d}} = [y_{\mathrm{d},0}, \cdots, y_{\mathrm{d},N-1}]^T \in \mathbb{C}^N \tag{17}$$
$$= \mathbf{U}^T\mathbf{y} \tag{18}$$
$$= \sqrt{\alpha E_0}\mathbf{\Lambda}\mathbf{Q}\mathbf{s} + \boldsymbol{\eta}_{\mathrm{u}}. \tag{19}$$

Furthermore, the ith substream of $\mathbf{y}_{\mathrm{d}}$ is formulated by

$$y_{\mathrm{d},i} = \sqrt{\alpha E_0}\lambda_i\sqrt{q_i}s_i + \eta_{\mathrm{u},i}, \tag{20}$$

where the equivalent average signal-to-noise ratio (SNR) is calculated by

$$\gamma_i = \frac{\mathbb{E}\left[\left|\sqrt{\alpha E_0}\lambda_i\sqrt{q_i}s_i\right|^2\right]}{\mathbb{E}\left[\left|\eta_{\mathrm{u},i}\right|^2\right]} \tag{21}$$
$$= \frac{\alpha E_0\lambda_i q_i}{N_0}. \tag{22}$$

C. Derivation of Optimal PA Coefficients

We derive the optimal PA matrix $\mathbf{Q}$ of the proposed scheme, by maximizing the capacity with the aid of the Lagrange multiplier method. Since the additive noises $\boldsymbol{\eta}_{\mathrm{u}}$ in (19) are uncorrelated, mutual information of the proposed scheme is upper-bounded by [17]

$$I(\mathbf{s};\mathbf{y}_{\mathrm{d}}) \leq \sum_{i=0}^{N-1}\log_2\left(1+\frac{\alpha E_0\lambda_i q_i}{N_0}\right) \text{ [bits/frame]}. \tag{23}$$

The transmit energy per frame in the conventional EVD-precoded NOFDM scheme without PA is given by

$$E_N = \mathbb{E}\left[\int_{-\infty}^{\infty}|x(t)|^2dt\right] \tag{24}$$
$$= \alpha E_0\mathbb{E}\left[\mathbf{x}^H\mathbf{H}\mathbf{x}\right] \tag{25}$$
$$= \alpha E_0\mathbb{E}\left[\mathbf{s}^H\mathbf{\Lambda}\mathbf{s}\right] \tag{26}$$
$$= \alpha E_0\sum_{i=0}^{N-1}\lambda_i\mathbb{E}\left[|s_i|^2\right] \tag{27}$$
$$= \alpha E_0 N, \tag{28}$$

where $\sum_{i=0}^{N-1}\lambda_i = \mathrm{trace}\{\mathbf{H}\} = N$ since each diagonal element of $\mathbf{H}$ is unity. Furthermore, the transmit energy per frame in the proposed scheme is calculated by

$$\bar{E}_N = \mathbb{E}\left[\int_{-\infty}^{\infty}|x(t)|^2dt\right] \tag{29}$$
$$= \alpha E_0\mathbb{E}\left[\mathbf{s}^H\mathbf{Q}\mathbf{U}^T\mathbf{H}\mathbf{U}\mathbf{Q}\mathbf{s}\right] \tag{30}$$
$$= \alpha E_0\mathbb{E}\left[\mathbf{s}^H\mathbf{Q}\mathbf{\Lambda}\mathbf{Q}\mathbf{s}\right] \tag{31}$$
$$= \alpha E_0\sum_{i=0}^{N-1}\lambda_i q_i\mathbb{E}\left[|s_i|^2\right] \tag{32}$$
$$= \alpha E_0\sum_{i=0}^{N-1}\lambda_i q_i. \tag{33}$$

In order to maintain the transmit energies of the two schemes to be equal, we arrive at the following constraint:

$$\bar{E}_N = E_N \tag{34}$$
$$\Leftrightarrow \sum_{i=0}^{N-1}\lambda_i q_i = N. \tag{35}$$

Next, in order to obtain the optimal q_i values, mutual information of (23) is maximized with respect to q_i, while satisfying the energy constraint of (35). Let us consider the following Lagrange function:

$$J = \sum_{i=0}^{N-1}\log_2\left(1+\frac{\alpha E_0\lambda_i q_i}{N_0}\right) - \xi\left(\sum_{i=0}^{N-1}\lambda_i q_i - N\right), \tag{36}$$

where ξ is the Lagrange multiplier. Here, to maximize J with respect to q_i, we consider

$$\frac{\partial J}{\partial q_i} = 0, \text{ subject to } q_i \geq 0, \tag{37}$$

yielding

$$q_i = \frac{1}{\lambda_i}. \tag{38}$$

Note that (38) satisfies the condition of $q_i \geq 0$ in (37), since $\lambda_i > 0$ is guaranteed. Hence, in the proposed scheme, it is ensured that each substream encounters the identical equivalent SNR of $\gamma_0 = \cdots = \gamma_{N-1} = \alpha E_0/N_0$ in (22).

D. Capacity of the Proposed Scheme

The capacity of the proposed scheme is maximized by substituting (38) into (23), which is formulated by

$$I(\mathbf{s};\mathbf{y}_{\mathrm{d}}) \leq \sum_{i=0}^{N-1}\log_2\left(1+\frac{\alpha E_0}{N_0}\right) \tag{39}$$
$$= N\log_2\left(1+\frac{\alpha E_0}{N_0}\right)[\text{bits/frame}]. \tag{40}$$

Also, the capacity normalized by the frame duration is given by

$$C_{\mathrm{F,opt}} = \frac{1}{T}I(\mathbf{s};\mathbf{y}_{\mathrm{d}}) \tag{41}$$
$$= \frac{N}{T}\log_2\left(1+\frac{\alpha E_0}{N_0}\right) \text{ [bps]}. \tag{42}$$

The capacity normalized by the bandwidth W is given by

$$\bar{C}_{\mathrm{F,opt}} = \frac{C_{\mathrm{F,opt}}}{W} \tag{43}$$
$$= \frac{N\log_2\left(1+\frac{\alpha E_0}{N_0}\right)}{(N-1)\alpha+1+\beta+\epsilon}\ [\text{bps/Hz}]. \tag{44}$$

Moreover, under the assumption of $N\alpha \gg 1$, (44) is simplified to

$$\bar{C}_{\mathrm{F,opt}} = \frac{1}{\alpha}\log_2\left(1+\frac{\alpha E_0}{N_0}\right)[\text{bps/Hz}]. \tag{45}$$

As formulated in (44), the capacity of the proposed scheme with optimal PA is given in a closed-form, which does not

include the eigenvalues λ_i, owing to the relationship of (38). Additionally, in the OFDM case ($\alpha = 1$), (44) corresponds to the classic Shannon capacity in the AWGN channel.

Moreover, we formulate the capacity in the limit of $\alpha \to 0$, by applying l'Hôpital's rule to (45), we arrive at

$$\lim_{\alpha \to 0} \bar{C}_{\mathrm{F,opt}} = \lim_{\alpha \to 0} \frac{\frac{\partial}{\partial \alpha} \log_2 \left(1 + \frac{\alpha E_0}{N_0}\right)}{\frac{\partial}{\partial \alpha} \alpha} \tag{46}$$

$$= \frac{1}{\ln 2} \cdot \frac{E_0}{N_0} \quad [\mathrm{bps/Hz}]. \tag{47}$$

III. Analytical Performance Results

Figs. 1(a) and 1(b) show the capacities of the conventional EVD-precoded NOFDM scheme without PA and the proposed EVD-precoded NOFDM scheme with optimal PA, respectively, each employing the RRC shaping filter with the roll-off factor of $\beta = 0.22$. The compression factor was given by $\alpha = 1.0, 0.5, 0.2, 0.1, 0.05$, and 0.01. The frame duration and the energy factor were set to $T = 1$ and $E_0 = 1$, respectively. The benchmark curve associated with the classic OFDM based on a rectangular pulse was also plotted. Observe in Fig. 1(a) that the conventional EVD-precoded NOFDM scheme with $\alpha < 1$ exhibited a higher capacity than the OFDM counterpart. More specifically, upon decreasing the compression factor α, its performance gain over OFDM increased. In Fig. 1(b), it was found that the proposed EVD-precoded NOFDM scheme with optimal PA achieved a significantly high capacity, which outperforms the conventional EVD-precoded NOFDM without PA and the OFDM. Furthermore, upon decreasing the compression factor, the capacity of the proposed scheme asymptotically approached the limit of $\alpha \to 0$ in (47).

IV. BER Results

In this section, we provide our BER performance results based on the Monte Carlo simulations. We considered the three-stage serially concatenated turbo-coded architecture. At the transmitter, information bits are encoded by a half-rate recursive systematic coding (RSC) encoder, and the RSC-encoded bits are interleaved by an outer interleaver Π_1. Then, the interleaved bits are encoded by the unity-rate coding (URC) encoder. Furthermore, the URC-encoded bits are interleaved again by an inner interleaver Π_2, in order to have the channel-encoded bits. At the receiver, extrinsic information in the form of log-likelihood ratios (LLRs) is exchanged between the three soft decoders, i.e., the LLR calculator, URC decoder, and the RSC decoder. The number of inner iterations and that of outer iterations are denoted I_{in} and I_{out}, respectively.

In our simulations, the number of subcarriers in NOFDM was maintained to be $N = 1000$, and the interleaver length was given by 20000. Therefore, a total of 20000 channel-encoded bits were transmitted by 20 NOFDM frames in each Monte Carlo simulation. As mentioned, in this paper, the effects of inter-frame interference were ignored, such that $\epsilon = 0$. The number of inner iterations and that of outer iterations were set to $I_{\mathrm{in}} = 2$ and $I_{\mathrm{out}} = 40$, respectively. Moreover, the normalized transmission rate R is calculated by

$$R = \frac{1}{2} \cdot \frac{\sum_{i=0}^{N-1} R_i}{(N-1)\alpha + (1 + \beta + \epsilon)} \ [\mathrm{bps/Hz}], \tag{48}$$

where R_i denotes the bit rate of the ith subcarrier.

Fig. 2 compares the bit-error ratios (BERs) of the proposed EVD-precoded NOFDM scheme with optimal PA and the conventional EVD-precoded NOFDM scheme without PA, each employing BPSK, where the roll-off factor of an RRC filter was given by $\beta = 0.22$. The compression factor was set to $\alpha = 0.5, 0.25, 0.125$, and 0.1, which corresponded to the normalized transmission rate of $R = 1.00, 1.99, 3.97$, and 4.94 [bps/Hz], respectively. For comparison, we also plotted the BER curves of the classic OFDM benchmark scheme, employing QPSK, 16-QAM, 256-QAM, and 1024-QAM, which exhibited the rates similar to those of the proposed and conventional NOFDM schemes. Also, the capacities associated with the three schemes were shown in each transmission rate, which corresponded to those in Figs. 1(a) and 1(b). Since the eigenvalues were sufficiently high in the simulated range of $0.1 \leq \alpha \leq 0.5$, truncation does not have to be activated in the proposed scheme. Observe in Fig. 2 that the proposed scheme outperformed the conventional NOFDM and the OFDM schemes for $R \geq 2$ [bps/Hz], as expected from the capacity results (Figs. 1(a) and 1(b)). The performance gain increased upon increasing the transmission rate of R. By contrast, the conventional EVD-precoded NOFDM scheme failed to outperform the OFDM benchmark for each R scenario. This is caused by the detrimental effects of low channel gains associated with low eigenvalues.

V. Conclusions

This paper proposed the novel EVD-precoded NOFDM with optimal PA. Based on the eigenvalue-decomposed independent parallel substreams, the capacities of the conventional and proposed EVD-precoded NOFDM schemes were derived as the extension of the classical OFDM capacity. The derived capacity was used for optimizing the PA coefficients of the proposed scheme. Our theoretical capacity analysis, as well as BER simulations, showed that the proposed scheme achieves higher performance than the conventional NOFDM scheme and the classic OFDM.

Acknowledgement

The present study was supported in part by the Japan Society for the Promotion of Science (JSPS) KAKENHI (Grant Numbers 16KK0120, 17H03259, 17K18871), and in part by JST PRESTO (Grant Number JPMJPR1933).

References

[1] W. Kozek and A. F. Molisch, "Nonorthogonal pulseshapes for multicarrier communications in doubly dispersive channels," *IEEE Journal on Selected Areas in Communications*, vol. 16, no. 8, pp. 1579–1589, Oct. 1998.

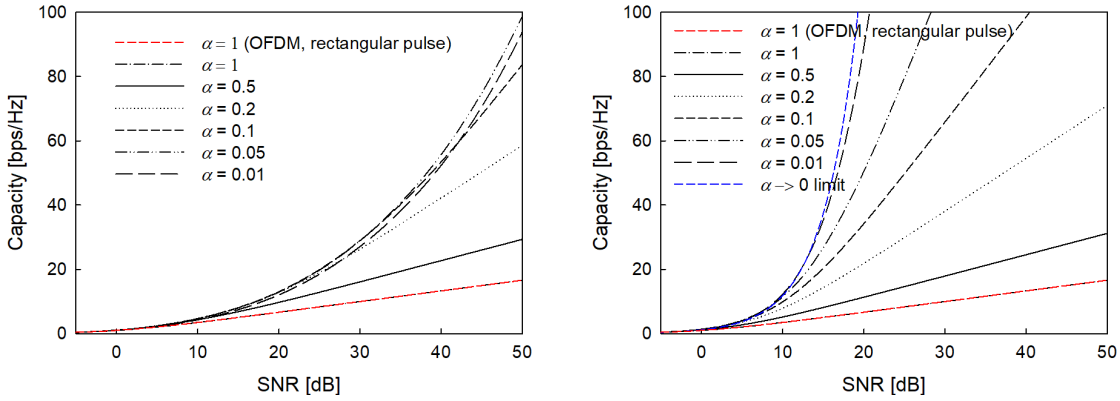

(a) Conventional EVD-precoded NOFDM

(b) Proposed EVD-precoded NOFDM

Fig. 1. Capacities of (a) the conventional EVD-precoded NOFDM scheme without PA and (b) the proposed EVD-precoded NOFDM scheme with optimal PA, each employing the RRC shaping filter with a roll-off factor of $\beta = 0.22$. The compression factor was given by $\alpha = 1.0, 0.5, 0.2, 0.1, 0.05$, and 0.01. The frame duration and the energy per subcarrier were fixed to $T = 1$ and $E_0 = 1$, while the number of the NOFDM subcarriers was fixed to $N = 1000$.

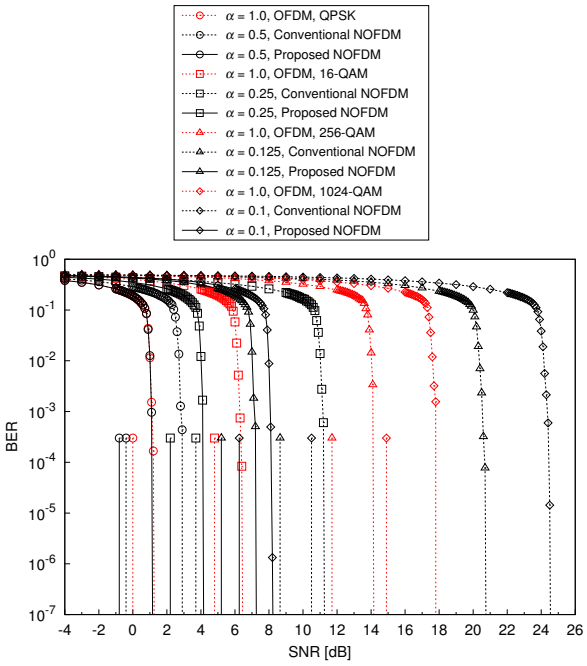

Fig. 2. BER comparisons of the proposed EVD-precoded NOFDM scheme with optimal PA, the conventional EVD-precoded NOFDM scheme without PA, and the classic OFDM. The compression factor was set to $\alpha = 0.5, 0.25, 0.125$, and 0.1, while maintaining the roll-off factor of $\beta = 0.22$.

[2] A. Kliks, H. Bogucka, I. Stupia, and V. Lottici, "A pragmatic bit and power allocation algorithm for NOFDM signalling," in *IEEE Wireless Communications and Networking Conference*, Budapest, Hungary, Apr. 2009, pp. 1–6.

[3] N. Michailow, M. Matthe, I. S. Gaspar, A. N. Caldevilla, L. L. Mendes, A. Festag, and G. Fettweis, "Generalized frequency division multiplexing for 5th generation cellular networks," *IEEE Transactions on Communications*, vol. 62, no. 9, pp. 3045–3061, Sept. 2014.

[4] I. Darwazeh, T. Xu, T. Gui, Y. Bao, and Z. Li, "Optical SEFDM system; bandwidth saving using non-orthogonal sub-carriers," *IEEE Photonics Technology Letters*, vol. 26, no. 4, pp. 352–355, Feb. 2014.

[5] S. V. Zavjalov, S. V. Volvenko, and S. B. Makarov, "A method for increasing the spectral and energy efficiency SEFDM signals," *IEEE Communications Letters*, vol. 20, no. 12, pp. 2382–2385, Dec. 2016.

[6] L. Hanzo, M. Münster, B. Choi, and T. Keller, *OFDM and MC-CDMA for Broadband Multi-User Communications, WLANs and Broadcasting*. John Wiley and IEEE Press, 2003.

[7] J. Huang, Q. Sui, Z. Li, and F. Ji, "Experimental demonstration of 16-QAM DD-SEFDM with cascaded BPSK iterative detection," *IEEE Photonics Journal*, vol. 8, no. 3, pp. 1–9, June 2016.

[8] Z. Li, F. Li, S. Qi, J. Li, J. Zhou, X. Yi, and Z. Li, "Beyond 100 Gb/s SEFDM signal IM/DD transmission utilizing TDE with 20% bandwidth compression," *IEEE Communications Letters*, vol. 23, no. 11, pp. 2017–2021, Nov. 2019.

[9] Y. Wang, Y. Zhou, T. Gui, K. Zhong, X. Zhou, L. Wang, A. P. T. Lau, C. Lu, and N. Chi, "Efficient MMSE-SQRD-Based MIMO decoder for SEFDM-based 2.4-Gb/s-spectrum-compressed WDM VLC system," *IEEE Photonics Journal*, vol. 8, no. 4, pp. 1–9, Aug. 2016.

[10] H. Ghannam, D. Nopchinda, M. Gavell, H. Zirath, and I. Darwazeh, "Experimental demonstration of spectrally efficient frequency division multiplexing transmissions at E-Band," *IEEE Transactions on Microwave Theory and Techniques*, vol. 67, no. 5, pp. 1911–1923, May 2019.

[11] S. Isam and I. Darwazeh, "Precoded spectrally efficient FDM system," in *21st Annual IEEE International Symposium on Personal, Indoor and Mobile Radio Communications*, Sept. 2010, pp. 99–104.

[12] D. Rainnie, Y. Feng, and J. Bajcsy, "On capacity merits of spectrally efficient FDM," in *IEEE Military Communications Conference*, Tampa, FL, USA, Oct. 2015, pp. 581–586.

[13] F. Rusek and J. B. Anderson, "Constrained capacities for faster-than-Nyquist signaling," *IEEE Transactions on Information Theory*, vol. 55, no. 2, pp. 764–775, Feb. 2009.

[14] A. Prlja and J. B. Anderson, "Reduced-complexity receivers for strongly narrowband intersymbol interference introduced by faster-than-Nyquist signaling," *IEEE Transactions on Communications*, vol. 60, no. 9, pp. 2591–2601, Sept. 2012.

[15] S. Sugiura, "Frequency-domain equalization of faster-than-Nyquist signaling," *IEEE Wireless Communications Letters*, vol. 2, no. 5, pp. 555–558, Oct. 2013.

[16] T. Ishihara and S. Sugiura, "Iterative frequency-domain joint channel estimation and data detection of faster-than-Nyquist signaling," *IEEE Transactions on Wireless Communications*, vol. 16, no. 9, pp. 6221–6231, Sept. 2017.

[17] T. Ishihara and S. Sugiura, "SVD-precoded faster-than-Nyquist signaling with optimal and truncated power allocation," *IEEE Transactions on Wireless Communications*, vol. 18, no. 12, pp. 5909–5923, Dec. 2019.

[18] K. Masaki, T. Ishihara, and S. Sugiura, "Effects of eigenvalue distribution on precoded faster-than-Nyquist signaling with power allocation," in *IEEE Vehicular Technology Conference (VTC2020-Fall)*, 4–7 Oct. 2020, pp. 1–5, in press.